Cell, Vol. 119, 369–380, October 29, 2004, Copyright ©2004 by Cell Press

The Pathway of HCV IRES-Mediated Translation Initiation

Geoff A. Otto[1] and Joseph D. Puglisi[2,*]
[1]Department of Microbiology and Immunology
[2]Department of Structural Biology
Stanford University School of Medicine
Stanford, California 94305

Summary

The HCV internal ribosome entry site (IRES) directly regulates the assembly of translation initiation complexes on viral mRNA by a sequential pathway that is distinct from canonical eukaryotic initiation. The HCV IRES can form a binary complex with an eIF-free 40S ribosomal subunit. Next, a 48S-like complex assembles at the AUG initiation codon upon association of eIF3 and ternary complex. 80S complex formation is rate limiting and follows the GTP-dependent association of the 60S subunit. Efficient assembly of the 48S-like and 80S complexes on the IRES mRNA is dependent upon maintenance of the highly conserved HCV IRES structure. This revised model of HCV IRES translation initiation provides a context to understand the function of different HCV IRES domains during translation initiation.

Introduction

An internal ribosome entry site (IRES) regulates translation of the hepatitis C virus (HCV) polyprotein (Tsukiyama-Kohara et al., 1992; Wang et al., 1993) in an essential, early step of viral replication. The 330 nt IRES, located in the 5′ untranslated region (UTR) of the 9500 nt HCV RNA genome, controls translation by a mechanism that is distinct from that for canonical mRNAs. The 5′ ^{7}meG-cap structure of a standard eukaryotic mRNA first assembles with eukaryotic initiation factor 4F (eIF4F). Subsequently, a 43S ribosomal complex, containing the 40S subunit, eIF3, ternary complex (eIF2·Met-tRNA$_i^{Met}$·GTP), and other factors, binds to eIF4F at the 5′ end and then scans the short (50–100 nt) 5′ UTR of the mRNA in an ATP-dependent manner to position the AUG in the ribosomal start site to form a transient 48S complex. Subsequent GTP-dependent release of initiation factors and 60S subunit joining, followed by first peptide bond formation, complete initiation of translation (reviewed in Hershey and Merrick [2000]).

HCV IRES-mediated translation initiation requires neither the 5′ cap structure nor ATP-dependent scanning and is predicted to require only a subset of the canonical initiation factors. The HCV IRES can direct internal initiation on a bicistronic mRNA construct (Tsukiyama-Kohara et al., 1992; Wang et al., 1993) by recruiting translation initiation complexes directly to the AUG start codon without scanning (Reynolds et al., 1996). Reconstitution of IRES initiation demonstrated that the IRES assembles on purified 40S subunits devoid of initiation factors (Pestova et al., 1998). The IRES·40S binary complex forms near the AUG codon; addition of only eIF3 and ternary complex docks the AUG in the ribosomal start site and yields a 48S-like (48S*) complex without eIF4F during the first step of translation (Hellen and Pestova, 1999). This model predicts a correlation that was not observed between IRES·40S binary complex affinity and translation activity (Kieft et al., 2001). Specifically, IRES mutations that efficiently form binary complexes can still have poor translation activity as compared to wild-type. Thus, the HCV IRES has additional functions during translation initiation that require maintenance of the HCV IRES structure.

The HCV sequence and secondary structure are highly conserved among viral isolates. The predicted IRES secondary structure is based upon phylogenetic comparison to the related pestiviruses and GB virus-B (Honda et al., 1999; Rijnbrand et al., 2000), chemical and enzymatic probing (Brown et al., 1992; Wang et al., 1995), and mutagenesis (Wang et al., 1994; Zhao and Wimmer, 2001). The HCV IRES contains two large helical domains (II and III) bridged by a pseudoknot to a short stem-loop domain (IV) that contains the initiation codon and a portion of the open reading frame. The structures of the HCV, pestivirus, and GB virus-B IRES motifs are similar with regions of absolute sequence conservation dispersed throughout unpaired regions of the secondary structure. Three-dimensional structures of IRES domains (Kieft et al., 2002; Lukavsky et al., 2000, 2003) have confirmed this secondary structure and provided atomic detail to IRES architecture.

The HCV IRES interacts with elements of the translation apparatus implicated in initiation complex recruitment, positioning, and regulation. Domain III mediates initial recruitment of the translation initiation complexes. The basal portion of domain III forms the core of the high-affinity interaction with the 40S subunit (Kieft et al., 2001; Kolupaeva et al., 2000; Lytle et al., 2001) and contacts ribosomal proteins that are involved in the binding and positioning of mRNA and tRNA (Otto et al., 2002). The apical portion of domain III (IIIb) interacts with eIF3 (Buratti et al., 1998; Kieft et al., 2001; Sizova et al., 1998), a multisubunit initiation factor involved in ternary complex stability and subunit assembly (reviewed in Hershey and Merrick [2000]). Domain II interacts with ribosomal protein S5 (Fukushi et al., 2001) and protrudes into the ribosomal start site, causing a conformational change in the 40S subunit (Spahn et al., 2001), suggesting roles in both mRNA and tRNA regulation. Proper positioning of the initiation codon is further controlled by the sequence (Fletcher et al., 2002) and stability (Honda et al., 1996) of domain IV. The interplay of these different putative IRES functions during initiation is not understood but likely involves regulation of initiation complex assembly. Further mechanistic studies of IRES-mediated translation are needed.

We present here analysis of HCV IRES-mediated initiation in complete translation systems. Our results show

*Correspondence: puglisi@stanford.edu

that the IRES directly regulates formation of both the 48S* and 80S translation initiation complexes and suggest a pathway for IRES-mediated translation initiation.

Results

Lack of Complete Correlation between IRES·40S Binding Affinity and IRES Translation Activity

The HCV IRES forms a high-affinity (dissociation constant, K_D = 2 nM) binary complex, which is relatively insensitive to IRES sequence, with purified HeLa 40S ribosomal subunits. The binding affinities for 40S subunits of mutant IRES transcripts, with changes in various conserved regions (Figure 1D), were measured by competition. Varying concentrations of unlabeled IRES transcripts were incubated with a wild-type IRES·40S complex formed between 0.5 nM ^{32}P end-labeled wild-type IRES and 0.5 nM HeLa 40S ribosomal subunits. Reactions were analyzed on native gels and quantitated on a phosphorimager to determine the binding affinity. A typical gel from a competition experiment with a domain II deletion mutant (dII-base, K_D = 6 nM) is shown in Figure 1A. The dissociation constants for other mutant constructs were similarly calculated and are summarized on the secondary structure of the IRES in Figure 1D. The stabilities of mutant 40S complexes are generally within an order of magnitude of the wild-type IRES·40S subunit dissociation constant (Kieft et al., 2001; Otto et al., 2002), with the exception of the double point mutant $A_{257/275}G$ (>50 nM).

The effects of RNA mutations on HCV IRES-mediated translation were determined by in vitro translation in lysates from HeLa S3 spinner cells (HeLa S10) and rabbit reticulocytes (RRL). Wild-type and mutant mRNA constructs consisted of the complete IRES attached in frame to the firefly luciferase open reading frame and terminated by the complete 3′ UTR of HCV (Kong and Sarnow, 2002). Translation activities were determined after a 40 min incubation at 30°C and quantitation of the ^{35}S-luciferase protein band resolved by SDS-PAGE. Translation of 100 nM wild-type IRES mRNA (Figure 1B) yields protein production between the initial lag phase and plateau at 40 min (Figure 1C). At higher IRES mRNA concentrations, a plateau in protein production was observed at earlier time points (data not shown). Similar results were observed in RRL (data not shown).

Evaluation of HCV IRES mutants in HeLa S10 and RRL revealed three different translation activity classes that correlate with the position of the mutation in the IRES secondary structure (Figure 1D). The mutants with the most severe defect in translation activity (i.e., no detectable luciferase in HeLa S10 and <10% of wild-type luciferase levels in RRL) all involve alterations in the basal portion of domain III. In this region, single-base changes in highly conserved regions, such as $A_{288}U$, are very deleterious, consistent with similar mutations tested in other systems (Kieft et al., 2001; Psaridi et al., 1999; Rijnbrand et al., 2000). Most of the severely impaired mutants have near wild-type binding affinity for 40S subunits. Intermediate translation activities (15% to 25% of wild-type protein production in HeLa S10 and RRL) were observed with either the truncation or substitution mutants of domain II, consistent with previous work on other domain II mutants (Honda et al., 1999; Zhao and Wimmer, 2001). The substitution mutants altered the highly conserved apical loop sequences by either replacing the loop-E motif with a helix (dII-delE) or substituting the apical loop with the UUCG tetraloop (dII-UUCG). The two most active mutants (>25% of wild-type protein production in HeLa S10 or RRL) involved the deletion of domain IIIb (del-IIIb) and a substitution to replace the loop-E motif in IIId with a helical segment (IIId-delE).

Sucrose Gradient Analysis of HCV IRES In Vitro Translation in HeLa S10

To understand better the mechanism of IRES-mediated translation, the assembly of HCV IRES mRNA into distinct translation complexes during HeLa S10 in vitro translation was monitored by sucrose density gradients. Sucrose gradients have been previously used to demonstrate that HCV IRES RNA bound purified 40S subunits (Pestova et al., 1998) and to separate distinct HCV translation complexes in RRL to map their RNase protection patterns (Lytle et al., 2001). To study the HCV IRES during HeLa S10 in vitro translation, ^{32}P body-labeled T7 transcribed HCV mRNA (described above) was incubated for 15 min at 30°C to ensure mRNA entry into the translation process. Translation reactions were quenched with chilled gradient buffer and loaded onto a 5%–20% sucrose gradient optimized for separation of 40S, 60S, and 80S translation components.

HCV IRES mRNA formed several complexes during translation in HeLa S10 extract as detected by sucrose gradients. These gradients were fractionated after passage through a UV detector; the lowest molecular weight species are at the top of the gradient (low elution volume). The UV absorbance profile (Figure 2A) has a large peak at the top of the gradient followed by three peaks corresponding to 40S, 60S, and 75S ribosomal particles. The 75S complex is formed by the mRNA-independent association of the 40S and 60S subunits (Safer et al., 1979). A similar profile was observed by plotting the total radioactivity measured for each gradient fraction. The source of the radioactivity in each fraction was first determined by Trizol extraction and denaturing urea PAGE analysis of each fraction. Good agreement was observed between the quantitation of full-length mRNA on the gel (Figure 2B) and the direct counting of the fractions (Figure 2A), except at the top of the gradient, which did not contain full-length mRNA. Gradient analysis of HCV IRES mRNA alone resulted in a single peak eluting at 3 ml, suggesting that the IRES was not aggregated under translation conditions (data not shown), consistent with the lack of aggregation observed by native gel analysis. The radioactivity detected at the top of the gradient likely arises from short RNA degradation products, whereas the radioactivity detected after 3 ml results from a complex of full-length HCV IRES mRNA and the translation apparatus.

The three peaks formed during active translation of the full-length HCV IRES mRNA in the HeLa S10 were identified as 80S, 40S, and 48S* complexes (Figure 2A). The limited resolution of these peaks could have been caused by partial degradation of the IRES mRNA but more likely reflects the low experimental sampling rate

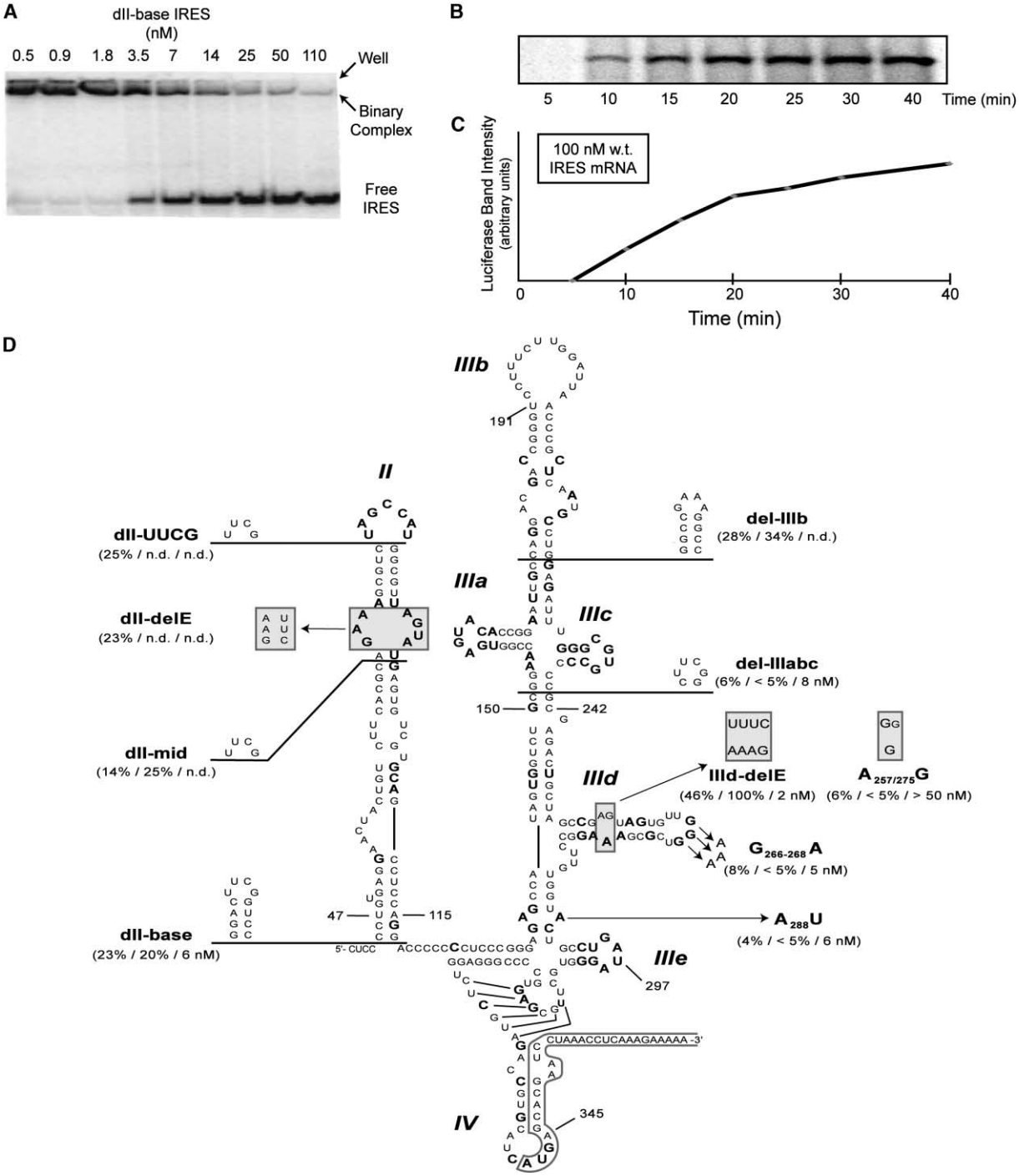

Figure 1. 40S Binding Affinity and Translation Activity of HCV IRES Mutants

(A) Autoradiograph of a 4% acrylamide native gel with 0.5 nM ^{32}P 5′-end-labeled wild-type HCV IRES and different concentrations of unlabeled dII-base mutant (from 0.5 to 110 nM) incubated with 5.5 nM HeLa 40S ribosomal subunits.

(B) Phosphorimager scan of a 12% SDS-PAGE gel of time points from HeLa S10 in vitro translation of 100 nM wild-type HCV IRES luciferase mRNA.

(C) Graph of luciferase protein band intensity versus time for the wild-type IRES.

(D) The HCV IRES secondary structure (Honda et al., 1999; Zhao and Wimmer, 2001; nt 40–370) is shown. The AUG and open reading frame are boxed. Nucleotides in bold are universally conserved with pestivirus structures (Hellen and Pestova, 1999). IRES mutants used in this study are indicated and include the relative translation efficiency from RRL/HeLa/and K_D (nM) in parentheses unless not determined (ND).

(points/ml) and continuing formation of unresolved translation intermediates (discussed below). The last peak to elute (10 ml) was identified as the IRES·80S complex. The intensity of this peak was enhanced by cycloheximide treatment in RRL (see below) and decreased under translation conditions where protein pro-

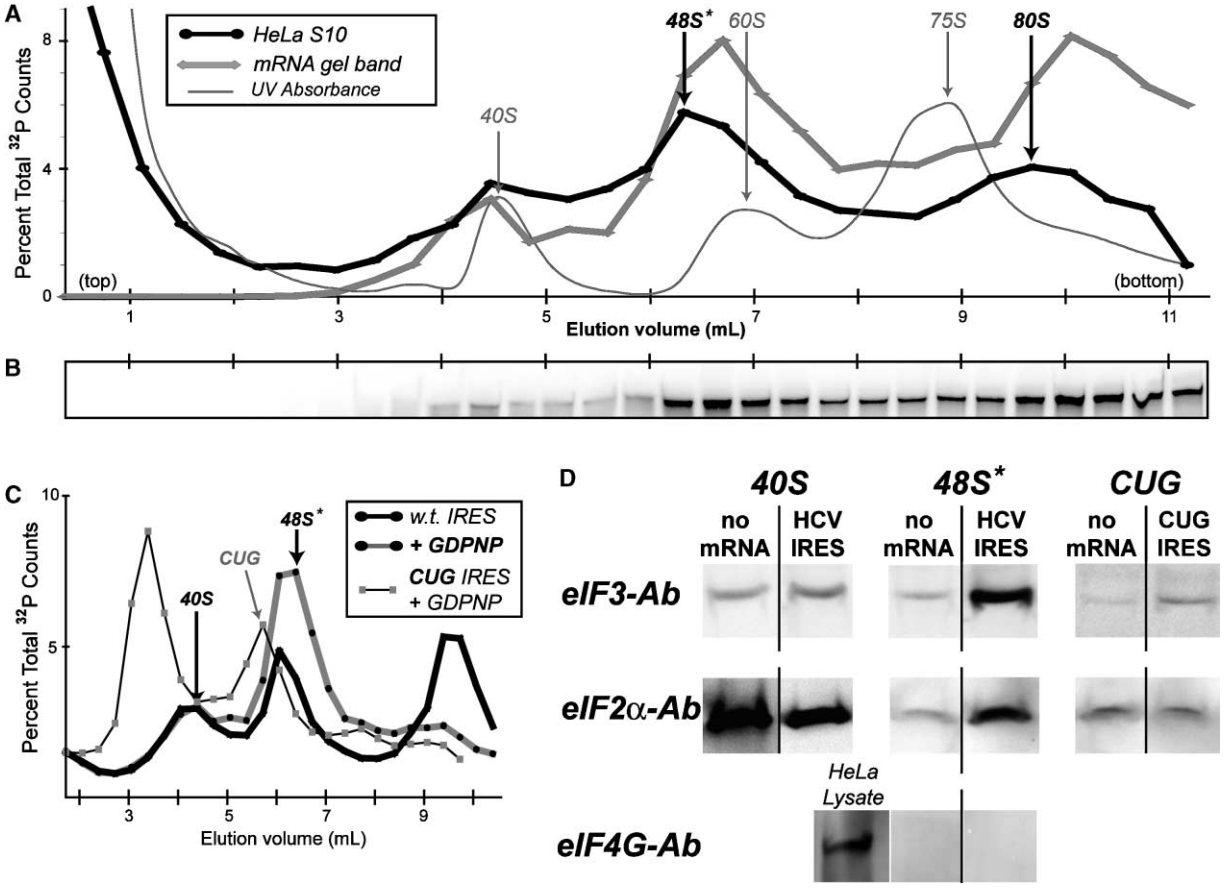

Figure 2. Sucrose Gradient Analysis of the HCV IRES in HeLa S10

(A) Graph of percent total radioactive counts versus elution volume for 5%–20% SW41 sucrose gradient analysis of a HeLa S10 in vitro translation reaction (15 min at 30°C) of 150 nM wild-type HCV IRES ^{32}P body-labeled mRNA (thick black, circles). The UV absorbance of the gradient is plotted to an arbitrary scale with the 40S, 60S, and 75S translation complexes labeled as a thin gray line.

(B) Phosphorimager scan of a 4% denaturing acrylamide gel cropped to show the full-length IRES mRNA region of Trizol-extracted sucrose gradient fractions of (A). Quantitation of band intensity is shown as thick gray with diamonds in (A).

(C) Graph of sucrose gradient analysis of $A_{342}C$ HCV IRES mRNA (thin black, gray squares) and wild-type IRES in the absence (thick black, circles) or presence of 1.7 mM GDPNP (thick gray, black circles) in HeLa S10.

(D) Phosphorimager scan of Western blot analysis of the 40S, 48S*, and CUG peaks in GDPNP-treated HeLa S10 gradients from translation reactions in the absence or presence of HCV IRES mRNA, as indicated in (C), with antibodies to eIF3-p66, eIF2α, and eIF4G (HeLa S10 sample included as a positive control).

duction was very poor (10 mM Mg^{2+} or 25°C, data not shown). The delayed elution of the active IRES mRNA·80S peak from the 75S UV peak likely reflects differences in complex composition. The IRES-containing mRNA·40S complex elutes at 4.5 ml. This complex was identified by reconstitution using highly purified 40S subunits (data not shown). A control luciferase mRNA lacking all of the HCV IRES elements did not form any of the mRNA peaks, consistent with the lack of protein production in HeLa S10 (data not shown).

Although the middle IRES mRNA peak at 6.5 ml cosediments with 60S subunits and 40S dimers, this species is not consistent with either an IRES·60S or 40S dimer complex. Formation of this peak was not effected by deletion of a putative 60S binding site in the 3′ UTR (Wood et al., 2001) of the IRES mRNA in HeLa S10 (data not shown) and was not reconstituted with purified 60S subunits (data not shown). The middle peak in HeLa S10 did not form in the presence of 10 mM Mg^{2+} (data not shown), which favors dimer formation, and was sensitive to changing the IRES initiation codon to a CUG ($A_{342}C$; Figure 2C) and other point mutants in the HCV IRES sequence (discussed below), suggesting that this species was not formed by 40S dimerization. The CUG mutant is inactive in protein synthesis and does not form 80S complexes (data not shown) but does form a complex of intermediate mobility between the IRES·40S and middle peaks.

The middle peak in the HeLa S10 sucrose gradient profiles was identified as a 48S* particle based upon GDPNP trapping and Western blots. The position of this peak suggested that it might correspond to a 48S* complex containing eIF3 and ternary complex (eIF2·Met-$tRNA_i^{Met}$·GTP), which may form during IRES-mediated translation initiation (Pestova et al., 1998). In a canonical 48S complex, hydrolysis of the ternary complex bound GTP is required for initiation factor release and subsequent 80S complex formation. Inhibition of this

step with GDPNP, a nonhydrolyzable GTP analog, blocks 80S formation, resulting in the accumulation of the 48S complex (reviewed in Hershey and Merrick [2000]). GDPNP treatment of the HeLa S10 programmed with HCV IRES mRNA blocked 80S formation and resulted in the buildup of the middle peak (Figure 2C), supporting its identification as an IRES·48S* complex.

Western blot analysis of the middle peak is consistent with its identification as a 48S* complex. After resolution by SDS-PAGE, fractions from this peak of GDPNP-treated HeLa S10 sucrose gradients in the absence or presence of HCV IRES mRNA were probed with antibodies to either the p66 subunit of eIF3, the α subunit of eIF2, or eIF4G (Figure 2D). The middle peak contains significantly greater amounts of both eIF3-p66 and eIF2α ($\sim$200% of control) compared to the no mRNA control and no detectable eIF4G. Similar analysis of a fraction from the 40S region revealed that the levels of eIF2α and eIF3-p66 were comparable in the absence or presence of the HCV IRES. The high levels of eIF2α observed likely reflect the failure to resolve the IRES·40S from the endogenous 43S complexes.

The intermediate peak of the IRES CUG initiation codon mutant had slightly more eIF3-p66 ($\sim$110% of control) but comparable levels of eIF2α, as compared to the no mRNA control in GDPNP-treated HeLa S10. The relative reduction in CUG eIF3-p66 blot intensity as compared to wild-type is consistent with the decreased peak size observed for CUG (Figure 2C). The CUG intermediate complex may contain eIF3 but lack eIF2.

The HCV IRES mRNA·40S and 48S* Complexes Are Intermediates during HeLa S10 In Vitro Translation

The kinetic pathway of HCV IRES-mediated translation initiation was analyzed by the timecourse of complex formation in HeLa S10. An analysis of early time points during in vitro translation in HeLa S10 suggests that both the HCV IRES·40S and IRES·48S* complexes are initiation intermediates. Six identical HeLa translation reactions were started simultaneously and then stopped after 1, 3, 6, 12, 18, or 24 min by dilution into chilled gradient buffer and storage on ice until gradient analysis (Figure 3A). Prolonged storage of other gradients under these conditions prior to gradient analysis did not significantly alter the complexes' profiles (data not shown), suggesting that these profiles reflect the state of the extract when translation was stopped. In this experiment, the large IRES·40S peak, initially observed at 1 min, steadily decreased in intensity at subsequent time points. The IRES·48S* peak first clearly formed at 3 min, increased in size at 6 min, and then decreased in size thereafter. The IRES·80S peak began to form at 6 min and increased in all subsequent time points. A similar timecourse performed in the presence of GDPNP also revealed that the IRES·40S peak formed first, followed by the IRES·48S*. 80S formation was blocked, and the levels of the 48S* peak were unchanged from 6 to 12 min (Figure 3B). A plot of peak volume versus time (Figure 3A, inset) clearly shows that the IRES·40S complex forms first, followed sequentially by the 48S* and then 80S complexes. Formation of the 80S complex from the 48S* requires GTP hydrolysis.

The HCV IRES Regulates Translation Initiation Complex Assembly

Mutations in the HCV IRES mRNA altered assembly of initiation complexes during in vitro translation in a HeLa lysate. Mutant and wild-type HCV IRES mRNA constructs were prepared and analyzed under identical conditions. The IRES mutants can be grouped into three translation activity classes (described above) that correlate with their different sucrose gradient profiles (Figure 4). Mutants with the most severe translation defects had an mRNA peak in the 40S, but not in the 48S* or 80S regions (Figure 4A). The intermediate-activity mutants, all involving alterations in domain II, formed mRNA peaks that were of similar size as for wild-type IRES (Figure 4B) in only the 40S and 48S* regions; no 80S species was observed. The small substitutions in the highly conserved apical loop (dII-UUCG) or apical internal loop (dII-delE) showed equivalent profiles as a partial (dII-mid) or complete truncation of domain II (data not shown). The two most active IRES mutant constructs, IIId-delE and del-IIIb, both had mRNA peaks in the 40S, 48S*, and 80S regions (Figure 4C). The lower relative level of 80S formation of del-IIIb compared to IIId-delE correlates with the relatively reduced protein production of this mutant.

The order of assembly of the 40S and 48S* complexes for the domain II deletion mutant (dII-mid) IRES is similar to that observed for wild-type; 80S complex formation is inhibited (Figure 3C). Only a large 40S peak was observed at 1 min, followed by the development of the 48S* at 3 min. Unlike the wild-type experiment, with dII-mid the 48S* peak continued to increase in size at the 6 and 12 min time points and no 80S peak ever developed. Thus, the domain II mutation represents a block in the transition from 48S* to 80S complex.

Differences Were Observed between the HCV IRES·48S* and Canonical 48S Complexes

As in HeLa S10, HCV IRES mRNA formed 48S* and 80S complexes during in vitro translation in RRL. Gradient analysis of RRL (Figure 5A) revealed a large radioactive peak at the top of the gradient followed by a very broad middle peak in the 40S to 60S UV region and a third peak in the 75S region. In RRL, the free 40S UV peak was smaller than that observed in untreated HeLa S10. The broad peak at the top of the gradient probably consists of degraded and free full-length IRES mRNA. The middle peak likely contains both the IRES·40S and IRES·48S* complexes. In RRL treated with GDPNP, a large 48S* peak that contained both eIF2α and eIF3-p66 was observed between 40S and 60S UV peaks, and no 80S peak was formed. Cycloheximide treatment enhanced the IRES·80S peak with a delayed elution compared to the 75S UV peak. The small differences in IRES peak mobility between HeLa S10 and RRL likely reflect differences in complex composition that are not required for efficient HCV IRES in vitro translation function.

Differences in the apparent lifetime and sucrose gradient mobility were observed between the HCV IRES mRNA·48S* and canonical 48S complexes formed on an uncapped luciferase mRNA (Figure 5B) despite comparable levels of overall protein production (data not

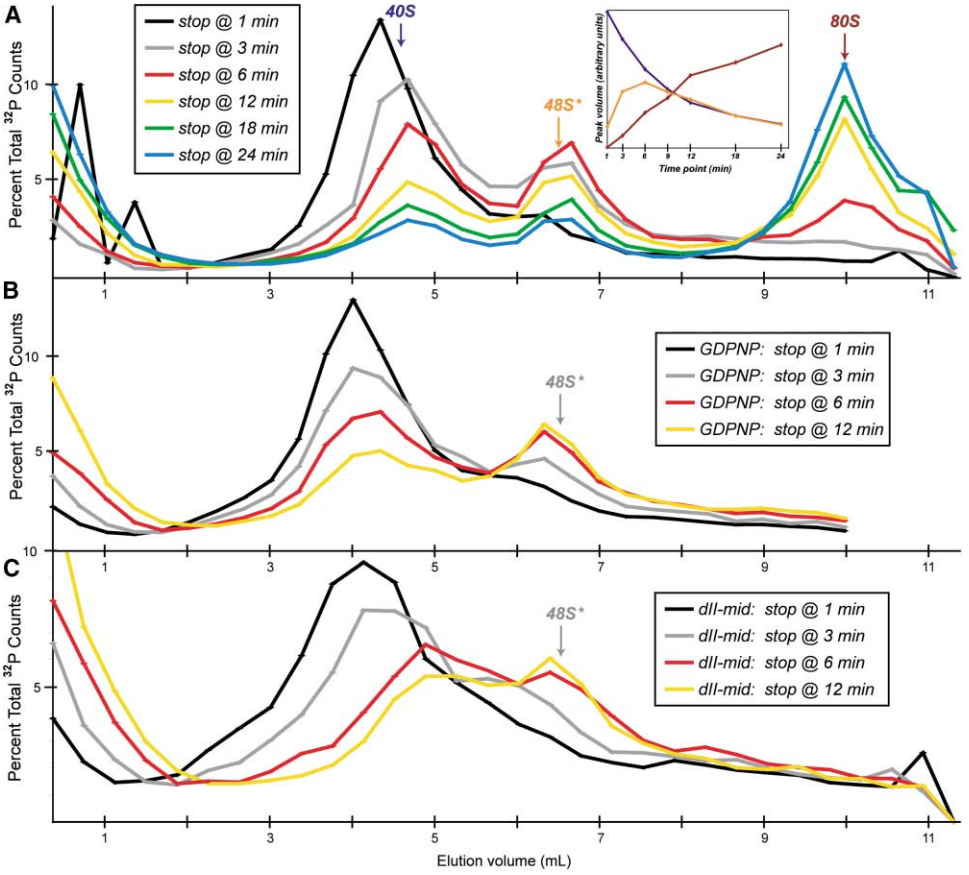

Figure 3. Timecourse of HCV IRES in HeLa Lysate Sucrose Gradients

(A) Graph of percent total radioactive counts versus elution volume for a timecourse of a HeLa S10 in vitro translation reaction at 30°C with 10 nM HCV IRES mRNA stopped at 1 (black), 3 (gray), 6 (red), 12 (yellow), 18 (green), or 24 (blue) min. Inset: Graph of 40S (blue), 48S* (orange), and 80S (brown) peak volume versus time.

(B) Graph of sucrose gradient analysis of a timecourse of HCV IRES mRNA in HeLa S10 treated with 1.7 mM GDPNP stopped at 1 (black), 3 (gray), 6 (red), and 12 (yellow) min.

(C) Graph of sucrose gradient analysis of a timecourse of dII-mid HCV IRES mRNA in HeLa S10 stopped at 1 (black), 3 (gray), 6 (red), and 12 (yellow) min.

shown). The luciferase mRNA forms only 80S complexes in untreated RRL; addition of GDPNP was required to observe the canonical 48S. In contrast, the IRES mRNA forms both the 48S* and 80S complexes in untreated RRL. The canonical GDPNP-dependent 48S migrated farther into the sucrose gradients than the IRES·48S* despite the smaller size of the luciferase mRNA (1700 nt versus 2300 nt), suggesting a difference in composition or conformation of these complexes. The canonical 48S contained eIF2α and eIF3-p66 but did not contain eIF4G, consistent with the expected composition of the canonical 48S (reviewed in Hershey and Merrick [2000]).

Positions of Ribosomal Complexes on HCV IRES mRNA in RRL Detected by Toeprinting

The sequence-dependent assembly of the HCV IRES mRNA into different translation initiation complexes in RRL was detected by inhibition of primer extension by reverse transcriptase (toeprinting). Primer extension stops, or toeprints, result from blocks of ^{32}P primer-directed reverse transcription that are sensitive to changes in secondary structure and RNA-ribosome interactions such that 48S and 80S complexes have different toeprint patterns (Dmitriev et al., 2003). Ribosomes positioned at the start codon (+1) cover the region downstream of canonical and HCV IRES (Pestova et al., 1998) mRNA, resulting in primer extension stops at the +16 and +17 positions. Toeprints of wild-type and mutant HCV IRES mRNA constructs in RRL (Figure 6) were detected on a sequencing gel using a ^{32}P primer in the luciferase open reading frame (nt 83 to 102) and are consistent with their behavior in the HeLa and RRL sucrose gradients.

Toeprint analysis of the wild-type IRES in RRL confirms the formation of 40S, 48S*, and 80S complexes. In untreated RRL, strong toeprints were visible at A_{357} and A_{358}, the positions +16 and +17 from the AUG, and in the pseudoknot at G_{318}, G_{320}, and U_{324} (Figure 6). There were also weaker stops at the start codon (A_{342} to G_{344}) and at U_{329}, A_{365}, and A_{371}. The stops in the pseudoknot region and at the AUG codon are consistent with toeprints previously observed in a wild-type IRES·40S complex (Pestova et al., 1998). Addition of GDPNP to RRL changed the toeprint pattern, reducing the intensity of

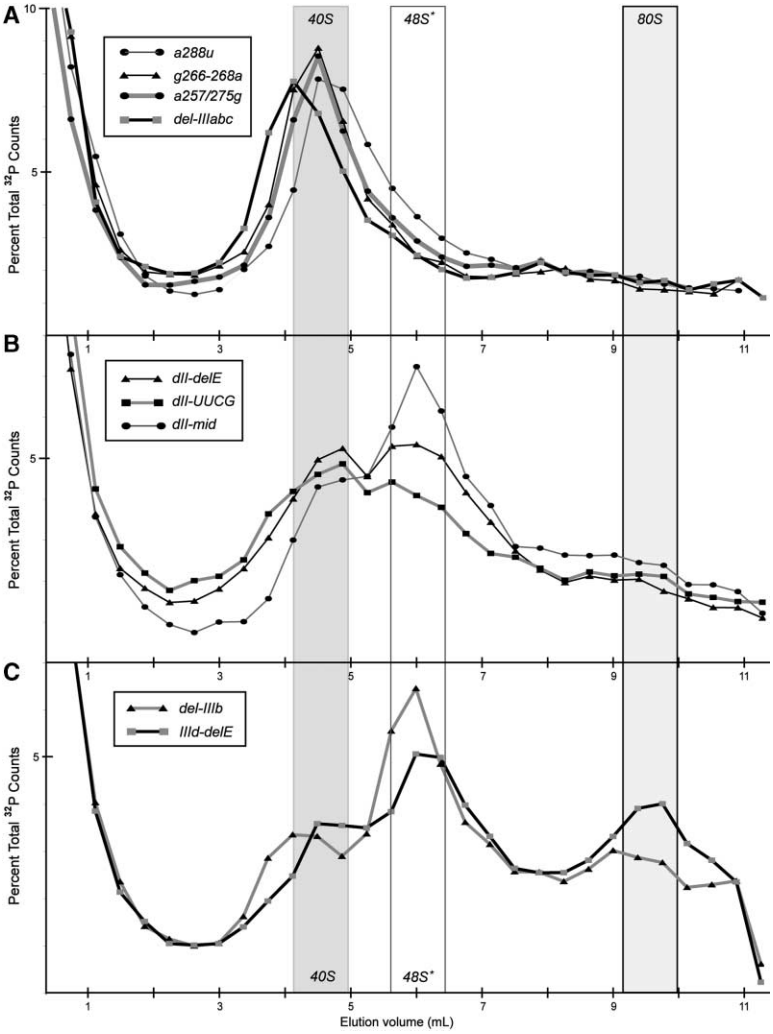

Figure 4. Sucrose Gradient Analysis of Mutant IRES mRNAs

(A) Graph of percent total radioactive counts versus elution volume for HeLa S10 in vitro translation reaction (15 min at 30°C) of 150 nM mutants IRES mRNAs with most severe translation defects, $A_{288}U$ (thin gray, black circles), $G_{266\text{-}268}A$ (thin black, triangles), $A_{257/275}G$ (thick gray, black circles), del-IIIabc (thick black, gray squares).

(B) Similar analysis of domain II mutants, dII-delE (thin black, triangles), dII-UUCG (thick gray, black squares), dII-mid (thin gray, black circles).

(C) Similar analysis of most translationally active mutant mRNAs, del-IIIb (gray, black triangles) and IIId-delE (black, gray squares).

the stops in the pseudoknot, AUG codon, and downstream of the strong +16 and +17 toeprints, which were unaltered. Similar toeprints were observed with a reconstituted 48S* complex, except that there was also an additional stop at A_{359}, +18 (Pestova et al., 1998). With cycloheximide treatment, a very strong stop at A_{358}, +17, and weak stops at A_{365} and A_{371} were observed. These IRES toeprints are similar to the strong +16–+18 and +17–+18 stops previously observed with two canonical mRNAs in RRL treated with GDPNP and cycloheximide, respectively (Dmitriev et al., 2003). Overall, there is a good agreement between the complexes observed in the RRL sucrose gradients (Figure 5A) and those detected by primer extension inhibition analysis. Toeprint experiments in HeLa S10 were unsuccessful, perhaps due to increased mRNA degradation in HeLa S10 as compared to RRL.

Primer extension inhibition of HCV IRES mutants in RRL reflected their behavior in sucrose gradients. Analysis of domain II mutants (dII-delE and dII-UUCG) revealed that in the presence of GDPNP, both mutants have a similar toeprint pattern to wild-type, but with a reduced intensity. Previously, a domain II deletion mutant (nt 26–67) also had a wild-type toeprint pattern of reduced intensity in a reconstituted 48S* complex (Pestova et al., 1998). These toeprints are consistent with the ability of these two mutant constructs to form a 48S* complex in GDPNP RRL sucrose gradients (data not shown). For two severely defective mutants, $A_{288}U$ and del-IIIabc, in cycloheximide-treated RRL, only very faint toeprints at +16 and +17 were observed relative to wild-type or the dII-delE mutant upon overexposure of the gel; consistently, these defective mutants are unable to form efficiently either 48S* or 80S complexes in RRL (data not shown) and HeLa S10. There was also a significant reduction in the G_{318} stop in the $A_{288}U$ mutant.

Discussion

The high-affinity binary complex formed between the HCV IRES and HeLa 40S subunit is not sufficient to explain IRES function during translation initiation. Mutation of universally conserved regions of the IRES caused severe defects in translation activity but only minor changes in binary complex affinity. Mutant IRES constructs with wild-type ($G_{266\text{–}268}A$) and significantly reduced ($A_{257/275}G$) binding affinity both have similar translation activity when expressed in mRNA constructs. The

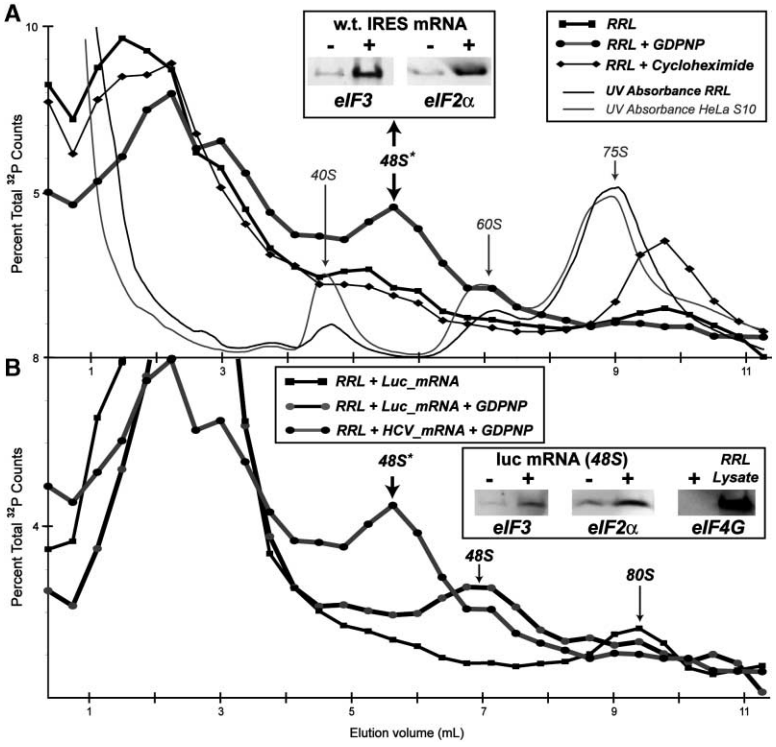

Figure 5. Sucrose Gradient Analysis of the HCV IRES in RRL

(A) Graph of percent total radioactive counts versus elution volume for untreated (thick black, squares) or 1 mM GDPNP-containing (thick gray, black circles) or 20 mM cycloheximide-containing (thin black, diamonds) RRL in vitro translation reaction (15 min at 30°C) of 100 nM wild-type HCV IRES ^{32}P body-labeled mRNA. The UV absorbance of RRL (black) and HeLa S10 (gray) is plotted to an identical arbitrary scale. Inset: Western blot analysis of the 48S* peak in GDPNP-treated RRL in the absence or presence of wild-type HCV IRES mRNA with antibodies to eIF3-p66 and eIF2α.

(B) Similar analysis of 100 nM uncapped luciferase mRNA in untreated (thick black, squares) and GDPNP-treated (thick black, gray circles) RRL with HCV IRES mRNA in GDPNP-treated RRL (thick gray, black circles). Inset: Western blot analysis of the 48S peak in GDPNP-treated RRL in the absence or presence of luciferase mRNA with antibodies to eIF3-p66, eIF2α, and eIF4G (mRNA versus RRL lysate control).

lack of complete correlation between affinity and activity indicates that the HCV IRES has additional regulatory functions during translation initiation beyond 40S association (Kieft et al., 2001).

Distinct translation initiation complexes assemble on an HCV IRES mRNA during in vitro translation in HeLa S10 and rabbit reticulocyte lysates. The initiation complexes were identified using sucrose gradients and verified by Western blots and primer extension inhibition. The HCV IRES formed 40S, 48S*, and 80S complexes in sucrose gradients from HeLa S10. Similar IRES mRNA complexes have been observed in ex vivo experiments using DNA-transfected 293T cells (Kong and Sarnow, 2002). This observation suggests that the formation of these complexes is not an artifact of the HeLa in vitro translation systems used here. In RRL, only 48S* and 80S complexes were observed. A distinct IRES·40S peak was not observed in the RRL sucrose gradients, but

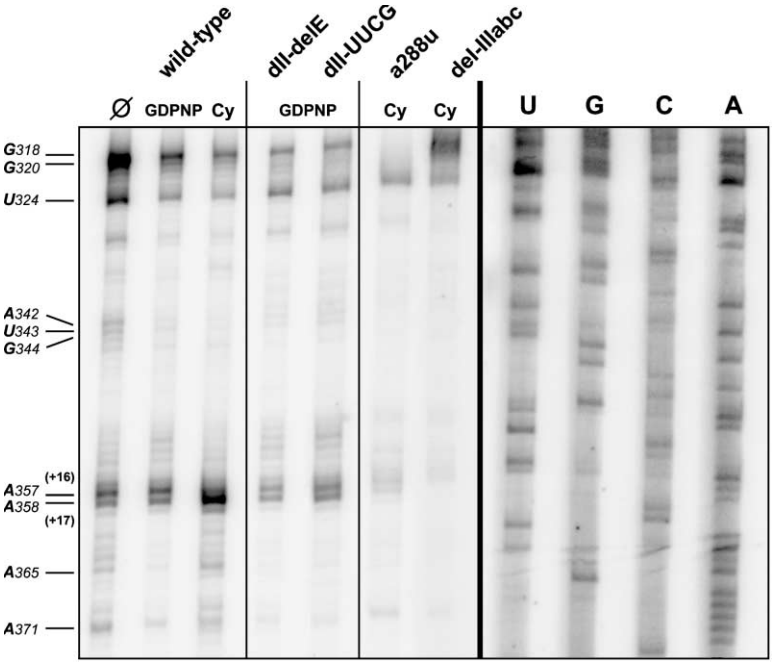

Figure 6. Primer Extension Inhibition of the HCV IRES mRNA in RRL

Phosphorimager scan of a 10% sequencing gel of toeprint reaction products from a ^{32}P end-labeled primer on wild-type, dII-delE, $A_{288}U$, and del-IIIabc mRNAs during in vitro translation in RRL that is untreated (Ø) or treated with GDPNP or cycloheximide (Cy) as indicated. Sequencing reactions were performed on free wild-type mRNA and used to determine the indicated nucleotide band locations.

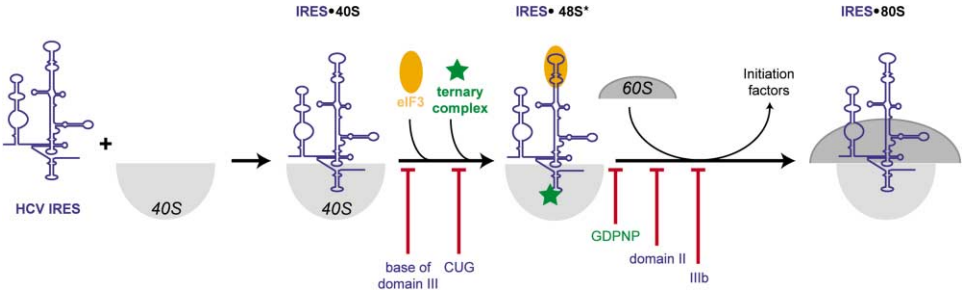

Figure 7. Model of HCV IRES Translation Initiation

The HCV IRES first binds to the 40S subunit and then eIF3 and ternary complex assemble to form a 48S* complex dependent upon both the base of domain III and proper initiation codon. Subsequent formation of the 80S complex is dependent upon GTP hydrolysis and 60S subunit joining and is regulated by domains II and IIIb of the IRES.

toeprints characteristic of this interaction were observed. The absence of a distinct IRES·40S peak in RRL is likely due to the lower concentration of free 40S subunits, as observed in the RRL UV absorbance profiles as compared to the HeLa lysates, and a large free mRNA peak that masks the 40S region.

The IRES·40S complex is a distinct intermediate formed during HCV IRES translation initiation. The IRES·40S peak in HeLa S10 has similar mobility to both the 40S UV peak and a reconstituted 40S·IRES complex formed from highly purified HeLa 40S subunits devoid of significant initiation factor contamination (Otto et al., 2002). This alignment suggests that the HeLa lysate IRES·40S complex does not contain initiation factors, consistent with the ability of the IRES to form a high-affinity binary complex with purified 40S subunits and the 40S toeprints observed in RRL. However, it is possible that the IRES·40S complex formed in HeLa S10 does contain eIF2, but not eIF3, given the high background levels of eIF2α detected in the 40S UV region.

The HCV IRES·48S* translation intermediate contains eIF2, eIF3, and the 40S ribosomal subunit, but not eIF4G, consistent with the 48S* complex predicted to form by Pestova et al. (1998). Western blot analysis of the 48S* complex in both HeLa S10 and RRL confirmed the presence of both eIF2α and eIF3-p66. Detection of p66 and eIF2α subunits likely indicates the presence of intact eIF3 and eIF2, respectively, in the IRES·48S* complex. eIF4G was not detected in the HeLa 48S* peak. In RRL, toeprints of the GDPNP-trapped 48S* are similar to those previously observed for reconstituted 48S* complexes (Pestova et al., 1998). An IRES mRNA with a CUG initiation codon formed an intermediate peak between the wild-type 40S and 48S* in HeLa sucrose gradients. The intermediate peak likely forms by addition of only eIF3 to the 40S since the intermediate peak had background levels of eIF2α, a component of the ternary complex. The mutated initiation codon could block ternary complex assembly and therefore 48S* formation (Pestova et al., 1998).

The HCV IRES mRNA begins translation as an IRES·40S complex then forms a 48S* intermediate prior to assembly of the 80S complex. Formation of these complexes, as monitored by sucrose gradient analyses of IRES translation timecourses, correlates with protein production and suggests a revised model for HCV IRES translation initiation (Figure 7). The HCV IRES enters the translation cycle by first binding to a 40S subunit that may contain eIF2 but does not contain eIF3. The IRES·40S complex then assembles with eIF3 and probably eIF2 to form a 48S* complex that is devoid of the cap binding factor. It is unknown if other initiation factors are present in the 48S*. In the 48S* complex, the IRES AUG initiation codon is properly paired with the anticodon of initiator tRNA in the ribosomal start site, as revealed by toeprinting. Transition of the 48S* intermediate to an 80S complex requires GTP hydrolysis, 60S subunit joining, and other unknown steps. In the previous model of HCV initiation, the IRES bound to a 40S subunit preassembled with both eIF3 and ternary complex to form the 48S* complex as the first step (Hellen and Pestova, 1999).

The formation, apparent lifetimes, and gradient mobility of the IRES·48S* intermediate are distinct from the canonical 48S complex. In canonical translation, eIF3 and ternary complex (eIF2·Met-tRNA$_i^{Met}$·GTP) are preassembled on the 40S subunit prior to the cap binding factor-dependent mRNA association to form a 43S complex that scans to the first start codon. The transient 48S complexes that are correctly positioned on the start codon rapidly progress to 80S complexes; canonical 48S complexes are only observed in the presence of GDPNP. In contrast, the IRES·48S* forms from the IRES·40S and does not require the cap binding factor. In GDPNP-treated RRL, the HCV 48S* complex had a lower gradient mobility compared to a 48S complex formed with a 600 nt shorter control luciferase mRNA. Lytle et al. (2001) also observed, but did not note, a similar shift between the IRES·48S* and β-globin·48S in RRL treated with the inhibitor edeine, suggesting that this difference is dependent upon the presence of the IRES and not on mRNA sequence. The distinct mobility of these complexes likely reflects differences in initiation factor composition other than eIF2, 3, or 4G. The canonical 48S is also predicted to contain eIF1, 1A, and 5, factors involved in start site selection and GTPase activation (reviewed in Hershey and Merrick [2000]). A more detailed analysis of the composition of the IRES·48S* is required to determine if these, or other, factors are present.

Progression from the 48S* to 80S initiation complexes is a slow step during IRES-mediated initiation causing the observed buildup of the 48S* peak. IRES·40S complexes form very rapidly, followed by buildup of the 48S* concentration within 1–5 min, and finally decrease of the 48S* intermediate and increase in 80S complexes.

A simple sequential mechanism for 40S→48S*→80S complex formation agrees with the observed time-course. This model is consistent with a 10-fold slower rate for the transition of 48S* to 80S complex (ca. 0.1 min^{-1}) than for the 40S to 48S* complex (ca. 1 min^{-1}). In contrast, in canonical translation the transition from 48S to 80S complex is rapid ($>>1$ min^{-1}) (Lorsch and Herschlag, 1999). The slow rate of 48S* to 80S transition may reflect decreased or absent factor activity or conformational rearrangements in the IRES leading to subunit joining.

Different domains of the HCV IRES regulate assembly of different initiation complexes during in vitro translation in RRL and HeLa S10. The functional roles of different IRES domains were assigned based on the behavior of IRES mutants in sucrose gradients and toeprint analysis. IRES mutants in the base of domain III were unable to form either 48S* or 80S complexes. Domain II mutants efficiently formed both the 40S and 48S* but not the 80S complexes. The deletion of domain IIIb enabled the IRES mRNA to form all three initiation complexes, but the 80S complex was not formed as efficiently as wild-type. After initial assembly of the IRES·40S complex, the basal portion of domain III controls assembly of initiation factors to form the 48S* complex (Figure 7). Domains II and IIIb regulate the subsequent formation of the 80S complex. These observations further support the proposed model of IRES initiation beginning with the 40S complex and provide a new means to understand the translation defects of these mutants.

48S* complex assembly is regulated by the base of domain III, which is the core of the 40S binding site (Kolupaeva et al., 2000). Most mutations in this region have little impact on 40S binding affinity but cause severe translation defects, consistent with their inability to progress beyond the first step in the pathway of IRES initiation. However, deletion of the loop-E motif in domain IIId (IIId-delE) had little effect on complex formation and translation activity, suggesting that the loop-E in IIId is not required for IRES function (Jubin et al., 2000). The regulatory function of the basal portion of the domain III region appears to occur prior to the assembly of any of the initiation factors on the 40S since intermediate complexes were not observed. Defective IRES mutants may bind to the surface of the 40S subunit with high affinity but fail to position the start codon correctly on the ribosome for 48S* complex formation. The altered toeprint patterns observed for $A_{288}U$ and del-IIIabc are indicative of the failure of these mutants to properly position the pseudoknot and domain IV regions on the 40S even though these mutants still bind to 40S subunits with high affinity.

Both domains II and IIIb are not required for 40S or 48S* assembly but regulate efficient 80S formation. Domain II is independently folded (Lukavsky et al., 2003) and protrudes into the decoding center of the 40S subunit, causing a conformational change that is predicted to close the mRNA channel (Spahn et al., 2001). Domain II also interacts with a ribosomal protein thought to be involved in tRNA positioning (Fukushi et al., 2001). Domain II mutants efficiently formed the 48S* complex at the same rates and comparable levels as wild-type; however, toeprint analysis of two of the mutants showed a reduction in the 48S* toeprints, as did a previous domain II mutant (Pestova et al., 1998). Therefore, domain II could regulate AUG position on the ribosome. Loss of this function should cause a reduction in the 48S* toeprint and inhibit 80S assembly without necessarily altering the composition and consequent gradient mobility of the 48S* complex. In addition, domain II may modulate the binding and activities of translation factors, specifically the GTPase activity of eIF2 or 5B, that mediate 48S* to 80S progression. The proposed regulation by domain II requires both the universally conserved hairpin and loop-E motif. The regulation of efficient 80S formation by IIIb is probably related to its known interaction with eIF3, an essential canonical initiation factor involved in ternary complex stabilization and subunit assembly (reviewed in Hershey and Merrick [2000]).

The revised model of HCV IRES-mediated translation initiation provides insights into IRES function and highlights the differences with canonical translation. The proposed differences in ternary complex recruitment could explain the differential sensitivity of HCV IRES and canonical translation to small changes in eIF2 levels or composition. In a previous study, a ribozyme reduced eIF2γ subunit mRNA levels by 20% and abrogated IRES activity with no apparent effect on canonical translation (Kruger et al., 2000). In addition, α-interferon, a poorly understood anti-HCV therapeutic, activates PKR (reviewed in He and Katze [2002]), a protein kinase that could differentially inhibit HCV and canonical translation initiation through phosphorylation of eIF2α.

The HCV IRES acts as a translation initiation factor directly regulating the assembly and functions of translation initiation complexes beginning with the 40S subunit. The IRES·40S binary complex forms a 48S* complex, which is distinct in composition from a canonical 48S complex, dependent upon the basal portion of domain III. An 80S complex forms if domain IIIb and the universally conserved loops in domain II are intact. This model provides the first detailed explanation for the translation defects observed in different IRES mutants and suggests new experiments to examine their functions in greater detail. These experiments also highlight the functional impact of single-nucleotide changes in this essential step in the HCV replication cycle, strengthening the validity of the HCV IRES as a potential therapeutic target. Finally, the simple techniques presented here can be applied to study the function of other viral and cellular IRES elements in greater detail.

Experimental Procedures

HCV IRES RNA Preparation

The IRES RNA (nt 40–370) used in the native gels was mutated, transcribed, and purified as described previously (Lukavsky et al., 2000; Otto et al., 2002). The full-length HCV IRES mRNA constructs were based upon a construct, generously provided by Drs. Li Kuo Kong and Peter Sarnow (Department of Microbiology and Immunology, Stanford University), that includes the complete HCV 5′ UTR plus 30 nt of the HCV core attached in frame to *Firefly* luciferase and terminated by the complete HCV 3′ UTR. mRNAs used in translation assays were purified by buffer exchange into water using an Amicon Ultra filter. HCV mRNAs for sucrose gradient analysis were body labeled (40 μCi ^{32}P α-ATP in a 50 μl reaction) and purified by G-50 gel filtration into water.

Native Gel Mobility Shift

The native gel mobility shift analysis of the HCV IRES (nt 40–370) was performed exactly as described previously (Otto et al., 2002).

0.5 nM ^{32}P-labeled wild-type IRES was incubated with 5.5 nM 40S subunits in the presence of increasing amounts of unlabeled mutant IRES constructs. Reaction products were analyzed on a 4% native gel and quantitated using a phosphorimager. Data were fit to a simple single-site binding equilibrium constant using Igor Pro. HeLa 40S and 60S ribosomal subunits were prepared using puromycin and 0.5 M KCl as described previously (Blobel and Sabatini, 1971; Otto et al., 2002).

HeLa S10 In Vitro Translation Extract Preparation

A 1 ml HeLa S3 (1 liter growth) cell pellet was obtained from the National Cell Culture Center. On ice, the pellet was diluted into 1.25 ml chilled hypotonic buffer (20 mM HEPES-KOH [pH 7.4], 15 mM NH_4Cl, 15 mM KOAc, 2.5 mM $MgOAc_2$, 0.1 mM hemin, 2 mM $CaOAc_2$, 2 mM DTT) in a small dounce homogenizer. After 10 min, 225 μl hypertonic buffer (100 mM HEPES-KOH [pH 7.4], 350 mM NH_4Cl, 350 mM KOAc, 1 mM EDTA, 500 mM sucrose, 10 mM ATP, 2 mM GTP, 100 mM creatine phosphate, 100 μg/ml CPK, 10 mM spermidine, 10 mM putrescine, 10 mM DTT) was added. The HeLa cells were lysed by 20 rapid strokes of the homogenizer and then spun at 22,000 × g for 30 min. The supernatant was stored in 200 μl aliquots at −80°C.

In Vitro Translation in RRL and HeLa S10

Translation reactions in nuclease-treated rabbit reticulocytes lysates (RRL) were performed as described in the instructions (Promega). These reactions were incubated at 30°C and included 50 nM IRES mRNA, 180 mM KCl, and 20 μCi ^{35}S Met. HeLa translation reactions were also incubated at 30°C and included 60% HeLa lysate, 150 nM IRES mRNA, 20 mM HEPES-KOH (pH 7.4), 180 mM KCl, 35 mM NH_4Cl, 1 mM $MgOAc_2$, 45 μM hemin, 45 mM sucrose, 1 mM ATP, 0.2 mM GTP, 10 mM Creatine phosphate, 10 μg/ml CPK, 1 mM spermidine, 1 mM putrescine, 1 mM $CaOAc_2$, 2 mM DTT, and 20 μCi ^{35}S Met. Aliquots of the translation reactions were RNase A treated, heated to 95°C for 5 min, and loaded on a 12% SDS-PAGE gel. The ^{35}S-luciferase bands on the gel were quantitated on a phosphorimager.

Sucrose Gradient Analysis of In Vitro Translation Reactions

Translation reactions (60 μl) from either HeLa S10 (45 μl HeLa lysate, 1.5 μl Superase·In [Ambion], 180 mM KOAc, 150 nM mRNA) or RRL (45 μl nuclease-treated RRL, 2 μl amino acids [Leu], 180 mM KOAc, 50 nM mRNA) were analyzed on 5% to 20% SW41 sucrose gradients in gradient buffer (50 mM HEPES-KOH [pH 7.4], 100 mM KOAc, 100 mM NH_4Cl, 10 mM $MgCl_2$, 2 mM DTT, 0.1 mM EDTA). The translation reactions were incubated as described in the text and quenched with 60 μl of chilled gradient buffer (0.4 mg/ml cycloheximide) and loaded onto the gradients and spun (37,000 rpm for 4 hr at 4°C). Gradients were analyzed using an ISCO UV detector and a Brandel, bottom-puncture syringe pump system. Gradients were fractionated (0.5 ml) and analyzed by Cerenkov counting.

Western Blots

Sucrose gradient fractions were TCA precipitated, resolved by SDS-PAGE, transferred to PVDF, blocked with 5% milk, and then blotted for eIF2α (ABCAM, ab5369), eIF3-p66 (PTG, 10219-1-AP), or eIF4G (Santa Cruz Biotech, sc-9601 or ABCAM, ab2609). Primary antibody binding was detected by enhanced chemifluorescence (ECF) on a phosphorimager using the appropriate alkaline phosphatase conjugated secondary antibody (Zymed).

Primer Extension Inhibition (Toeprinting)

Toeprinting was performed on the full-length HCV IRES mRNA in RRL incubated for 10 min at 30°C using a ^{32}P-labeled primer complementary to 83 to 102 of luciferase as described previously (Pestova et al., 1998). Reactions were resolved on a 10% sequencing gel and detected on a phosphorimager.

Acknowledgments

We thank Peter Sarnow and Sunny Choe for technical assistance, encouragement, and collaboration. This work was supported by NIH grant AI47365 and a grant from the Hutchison Foundation.

Received: April 26, 2004
Revised: September 2, 2004
Accepted: September 10, 2004
Published: October 28, 2004

References

Blobel, G., and Sabatini, D. (1971). Dissociation of mammalian polyribosomes into subunits by puromycin. Proc. Natl. Acad. Sci. USA *68*, 390–394.

Brown, E.A., Zhang, H., Ping, L.H., and Lemon, S.M. (1992). Secondary structure of the 5′ nontranslated regions of hepatitis C virus and pestivirus genomic RNAs. Nucleic Acids Res. *20*, 5041–5045.

Buratti, E., Tisminetzky, S., Zotti, M., and Baralle, F.E. (1998). Functional analysis of the interaction between HCV 5′UTR and putative subunits of eukaryotic translation initiation factor eIF3. Nucleic Acids Res. *26*, 3179–3187.

Dmitriev, S.E., Pisarev, A.V., Rubtsova, M.P., Dunaevsky, Y.E., and Shatsky, I.N. (2003). Conversion of 48S translation preinitiation complexes into 80S initiation complexes as revealed by toeprinting. FEBS Lett. *533*, 99–104.

Fletcher, S.R., Ali, I.K., Kaminski, A., Digard, P., and Jackson, R.J. (2002). The influence of viral coding sequences on pestivirus IRES activity reveals further parallels with translation initiation in prokaryotes. RNA *8*, 1558–1571.

Fukushi, S., Okada, M., Stahl, J., Kageyama, T., Hoshino, F.B., and Katayama, K. (2001). Ribosomal protein S5 interacts with the internal ribosomal entry site of hepatitis C virus. J. Biol. Chem. *276*, 20824–20826.

He, Y., and Katze, M.G. (2002). To interfere and to anti-interfere: the interplay between hepatitis C virus and interferon. Viral Immunol. *15*, 95–119.

Hellen, C.U., and Pestova, T.V. (1999). Translation of hepatitis C virus RNA. J. Viral Hepat. *6*, 79–87.

Hershey, J.W.B., and Merrick, W.C. (2000). The pathway and mechanism of initiation of protein synthesis. In Translation Control of Gene Expression, N. Sonenberg, J.W.B. Hershey, and M.B. Mathews, eds. (Cold Spring Harbor, NY: Cold Spring Harbor Laboratory Press), pp. 33–88.

Honda, M., Brown, E.A., and Lemon, S.M. (1996). Stability of a stem-loop involving the initiator AUG controls the efficiency of internal initiation of translation on hepatitis C virus RNA. RNA *2*, 955–968.

Honda, M., Beard, M.R., Ping, L.H., and Lemon, S.M. (1999). A phylogenetically conserved stem-loop structure at the 5′ border of the internal ribosome entry site of hepatitis C virus is required for cap-independent viral translation. J. Virol. *73*, 1165–1174.

Jubin, R., Vantuno, N.E., Kieft, J.S., Murray, M.G., Doudna, J.A., Lau, J.Y., and Baroudy, B.M. (2000). Hepatitis C virus internal ribosome entry site (IRES) stem loop IIId contains a phylogenetically conserved GGG triplet essential for translation and IRES folding. J. Virol. *74*, 10430–10437.

Kieft, J.S., Zhou, K., Jubin, R., and Doudna, J.A. (2001). Mechanism of ribosome recruitment by hepatitis C IRES RNA. RNA *7*, 194–206.

Kieft, J.S., Zhou, K., Grech, A., Jubin, R., and Doudna, J.A. (2002). Crystal structure of an RNA tertiary domain essential to HCV IRES-mediated translation initiation. Nat. Struct. Biol. *9*, 370–374.

Kolupaeva, V.G., Pestova, T.V., and Hellen, C.U. (2000). An enzymatic footprinting analysis of the interaction of 40S ribosomal subunits with the internal ribosomal entry site of hepatitis C virus. J. Virol. *74*, 6242–6250.

Kong, L.K., and Sarnow, P. (2002). Cytoplasmic expression of mRNAs containing the internal ribosome entry site and 3′ noncoding region of hepatitis C virus: effects of the 3′ leader on mRNA translation and mRNA stability. J. Virol. *76*, 12457–12462.

Kruger, M., Beger, C., Li, Q.X., Welch, P.J., Tritz, R., Leavitt, M., Barber, J.R., and Wong-Staal, F. (2000). Identification of eIF2B-gamma and eIF2gamma as cofactors of hepatitis C virus internal ribosome entry site-mediated translation using a functional genomics approach. Proc. Natl. Acad. Sci. USA *97*, 8566–8571.

Lorsch, J.R., and Herschlag, D. (1999). Kinetic dissection of fundamental processes of eukaryotic translation initiation in vitro. EMBO J. *18*, 6705–6717.

Lukavsky, P.J., Otto, G.A., Lancaster, A.M., Sarnow, P., and Puglisi, J.D. (2000). Structures of two RNA domains essential for hepatitis C virus internal ribosome entry site function. Nat. Struct. Biol. *7*, 1105–1110.

Lukavsky, P.J., Kim, I., Otto, G.A., and Puglisi, J.D. (2003). Structure of HCV IRES domain II determined by NMR. Nat. Struct. Biol. *10*, 1033–1038.

Lytle, J.R., Wu, L., and Robertson, H.D. (2001). The ribosome binding site of hepatitis C virus mRNA. J. Virol. *75*, 7629–7636.

Otto, G.A., Lukavsky, P.J., Lancaster, A.M., Sarnow, P., and Puglisi, J.D. (2002). Ribosomal proteins mediate the hepatitis C virus IRES-HeLa 40S interaction. RNA *8*, 913–923.

Pestova, T.V., Shatsky, I.N., Fletcher, S.P., Jackson, R.J., and Hellen, C.U. (1998). A prokaryotic-like mode of cytoplasmic eukaryotic ribosome binding to the initiation codon during internal translation initiation of hepatitis C and classical swine fever virus RNAs. Genes Dev. *12*, 67–83.

Psaridi, L., Georgopoulou, U., Varaklioti, A., and Mavromara, P. (1999). Mutational analysis of a conserved tetraloop in the 5′ untranslated region of hepatitis C virus identifies a novel RNA element essential for the internal ribosome entry site function. FEBS Lett. *453*, 49–53.

Reynolds, J.E., Kaminski, A., Carroll, A.R., Clarke, B.E., Rowlands, D.J., and Jackson, R.J. (1996). Internal initiation of translation of hepatitis C virus RNA: the ribosome entry site is at the authentic initiation codon. RNA *2*, 867–878.

Rijnbrand, R., Abell, G., and Lemon, S.M. (2000). Mutational analysis of the GB virus B internal ribosome entry site. J. Virol. *74*, 773–783.

Safer, B., Jagus, R., and Kemper, W.M. (1979). Analysis of initiation factor function in highly fractionated and unfractionated reticulocyte lysate systems. Methods Enzymol. *60*, 61–87.

Sizova, D.V., Kolupaeva, V.G., Pestova, T.V., Shatsky, I.N., and Hellen, C.U. (1998). Specific interaction of eukaryotic translation initiation factor 3 with the 5′ nontranslated regions of hepatitis C virus and classical swine fever virus RNAs. J. Virol. *72*, 4775–4782.

Spahn, C.M., Kieft, J.S., Grassucci, R.A., Penczek, P.A., Zhou, K., Doudna, J.A., and Frank, J. (2001). Hepatitis C virus IRES RNA-induced changes in the conformation of the 40s ribosomal subunit. Science *291*, 1959–1962.

Tsukiyama-Kohara, K., Iizuka, N., Kohara, M., and Nomoto, A. (1992). Internal ribosome entry site within hepatitis C virus RNA. J. Virol. *66*, 1476–1483.

Wang, C., Sarnow, P., and Siddiqui, A. (1993). Translation of human hepatitis C virus RNA in cultured cells is mediated by an internal ribosome-binding mechanism. J. Virol. *67*, 3338–3344.

Wang, C., Sarnow, P., and Siddiqui, A. (1994). A conserved helical element is essential for internal initiation of translation of hepatitis C virus RNA. J. Virol. *68*, 7301–7307.

Wang, C., Le, S.Y., Ali, N., and Siddiqui, A. (1995). An RNA pseudoknot is an essential structural element of the internal ribosome entry site located within the hepatitis C virus 5′ noncoding region. RNA *1*, 526–537.

Wood, J., Frederickson, R.M., Fields, S., and Patel, A.H. (2001). Hepatitis C virus 3′X region interacts with human ribosomal proteins. J. Virol. *75*, 1348–1358.

Zhao, W.D., and Wimmer, E. (2001). Genetic analysis of a poliovirus/hepatitis C virus chimera: new structure for domain II of the internal ribosomal entry site of hepatitis C virus. J. Virol. *75*, 3719–3730.